Journal of Power Sources 196 (2011) 10289–10296

Contents lists available at ScienceDirect

Journal of Power Sources

journal homepage: www.elsevier.com/locate/jpowsour

Characterization of all-solid-state Li/LiPONB/TiOS microbatteries produced at the pilot scale

B. Fleutot[a,b], B. Pecquenard[a,*], F. Le Cras[c], B. Delis[a], H. Martinez[d], L. Dupont[e], D. Guy-Bouyssou[b]

[a] CNRS, Université de Bordeaux, ICMCB site de l'ENSCBP, 87 Av du Dr. Schweitzer, Pessac F-33608, France
[b] STMicroelectronics, Advanced Technologies R&D, IMS/ASD & IPAD division, 16 rue Pierre et Marie Curie, B.P. 7155, 37071 Tours Cedex 2, France
[c] CEA LITEN, 17 rue des Martyrs, 38054 Grenoble, France
[d] Laboratoire IPREM – UMR 5254, Université de Pau et des Pays de l'Adour, Hélioparc Pau-Pyrénées, 2 Av du Président Angot, 64053 Pau Cedex 9, France
[e] LRCS – UMR 6007, Université de Picardie Jules Verne, 33 rue Saint Leu, 80039 Amiens, France

ARTICLE INFO

Article history:
Received 15 February 2011
Received in revised form 5 July 2011
Accepted 6 July 2011
Available online 18 July 2011

Keywords:
Lithium
Microbattery
Titanium oxysulfide
Thin films
LiPON

ABSTRACT

All-solid-state Li/LiPONB/TiOS microbatteries were manufactured at the pilot scale on silicon substrate. In a first attempt, the characterization of the active materials constituting the microbattery was achieved in order to determine their accurate composition, structure and morphology. Finally, a thorough electrochemical characterization was carried out on all-solid-state cells. Excellent performances were noted in terms of cycle life (with more than 1000 cycles), efficiency and self-discharge (less than 5% per year). In addition, the positive electrode highlighted a high volumetric capacity close to 90 $\mu Ah\,cm^{-2}\,\mu m^{-1}$ when cycled at 100 $\mu A\,cm^{-2}$ between 1 V and 3 V vs. Li^+/Li.

1. Introduction

The development and the miniaturization of portable electronic devices have stimulated numerous research projects in the field of micro-power sources. All-solid-state microbatteries are becoming an interesting alternative to button cells or conventional Li-ion cells in numerous applications (stand-alone sensors, energy backup for memories, RFID tags, etc.) for which these latter cells are oversized. The reduced footprint of microbatteries enables a wide range of integration modes, and in particular the opportunity to manufacture them directly onto microsystems.

An all-solid-state thin film battery can be defined as a monolithic system constituted of more than 10 layers including the active part (both electrodes and the electrolyte), protective layers, current collectors and thin film barriers, with a total thickness not exceeding 15 μm. The active materials of a microbattery can be fabricated by different methods including physical vapor deposition (PVD) techniques such as evaporation or sputtering, which are commonly used in the microelectronics industry. In these microbatteries, the use of a solid electrolyte, despite its low ionic conductivity, has numerous advantages. The most important ones are the possibility of using metallic lithium as a rechargeable negative electrode, the low reactivity at the electrode/electrolyte interface contributing to a very low self-discharge rate, and the possible operation at elevated temperatures. Moreover, the absence of a liquid electrolyte enhances the intrinsic safety of the battery, and has a particular interest for healthcare applications.

Various studies were carried out on all-solid-state lithium thin film batteries [1–4] based on metallic lithium as a negative electrode prepared by evaporation, lithium phosphorus oxynitride (LiPON) as a solid electrolyte prepared by sputtering from a Li_3PO_4 target under pure nitrogen gas and a positive electrode which strongly influences the characteristics of the whole system. Two types of positive electrodes can be considered. The first type concerns lithiated ones such as $LiCoO_2$ and $LiMn_2O_4$ which need to be thermally treated (400–700 °C) to get the performing crystalline structure. These materials operate reversibly around 4 V/Li^+/Li, and are directly synthesized in the discharged (reduced) state. The other type gathers transition metal oxides or sulfides such as V_2O_5, TiS_2, which can be directly synthesized in an amorphous state (or crystallized for V_2O_5) [4,5] without any additional annealing and reversibly insert lithium mainly below 3 V/Li^+/Li. Thus these latter materials need to be associated with a lithiated negative electrode. The performances of these different positive electrode materials associated with LiPON and metallic lithium are summarized in Table 1 [1].

* Corresponding author. Tel.: +33 5 40 00 33 03; fax: +33 5 40 00 66 98.
E-mail address: pecquen@icmcb-bordeaux.cnrs.fr (B. Pecquenard).

0378-7753/$ – see front matter © 2011 Elsevier B.V. All rights reserved.
doi:10.1016/j.jpowsour.2011.07.018

Table 1
Comparison of electrochemical performances of various positive electrodes in all-solid-state cells (positive electrode/LiPON/Li) according to Bates [1].

	c-$LiCoO_2$[a]	c-$LiMn_2O_4$[a]	V_2O_5	TiS_2
Capacity ($\mu Ah\,cm^{-2}\,\mu m^{-1}$)	62 [4.2–3.5 V]	40 [4.2–3.5 V]	123 [3.7–1.5 V]	75 [2.45–1.8 V]
Energy density ($Wh\,l^{-1}$)	400	433	611	364
Specific energy ($Wh\,kg^{-1}$)	200	211	444	225
Annealing	700 °C, O_2	400 °C, O_2	Without	Without

[a] c- means that the compound is crystallized.

In the present work, titanium oxysulfide thin films were selected because of their specific potential window [1.0–3.0 V/Li^+/Li] well-adapted for the envisaged application. For more than twenty years, this type of material has been thoroughly studied by the ICMCB group either with solid or liquid electrolytes [6,7]. Contrary to most of the published works concerning titanium disulfide, the thin films prepared by sputtering always contain some oxygen due to the strong avidity of titanium for oxygen (the oxygen coming from the target and/or the presence of remaining water molecules always present in the chamber whatever the initial vacuum). The incorporation of oxygen induces the presence of two types of sulfur species: S^{2-} as in TiS_2, and S_2^{2-} disulfide pairs as in TiS_3. These disulfides pairs present in TiO_yS_z can then be reduced at the beginning of the lithium insertion (i.e. at higher voltage) and contribute to an increase of the capacity of the positive electrode compared to pure TiS_2 [8]. So, for optimum performance, the TiO_yS_z thin films need to contain a large proportion of these disulfide pairs, since they play a large part in the redox processes together with titanium ions. Furthermore, a previous study led in a liquid electrolyte has highlighted the beneficial effect on the reversibility of the sulfur redox process of having a dense thin film [8].

Concerning the electrolyte, the addition of a few percents of boron into LiPON electrolyte is known to enhance its chemical and thermal stability while maintaining good electrical performances [9]. The latter, named LiPONB, was used in this study.

In the present work, we report on the development of Li/LiPONB/TiO_yS_z all-solid-state lithium microbatteries manufactured at the pilot scale, the characterization of the active materials constituting the microbattery (positive electrode and solid electrolyte) in order to determine their composition, structure and morphology and finally on the thorough study of their electrochemical performances.

2. Experimental procedure

2.1. TiO_yS_z thin film deposition

To avoid any contamination, the sputtering chamber is connected to an argon-filled glove box. Before deposition, a vacuum was created into the chamber until the pressure was less than 4×10^{-6} Pa. Prior to each deposition, a pre-sputtering was systematically carried out for 20 min. The titanium oxysulfide films were grown at room temperature with no intentional heating/cooling of the substrates. The reactive sputtering was held in DC mode with a Ti target in an Ar/O_2 atmosphere (1% O_2) with a constant gas flow of 16 sccm (partial pressure of 0.2 Pa) and a constant H_2S flow rate of 18 sccm (partial pressure of 0.2 Pa). For all samples, the incident power density was 2.5 W cm^{-2}. The growth rate of TiO_yS_z thin films was determined by profilometry equal to 3 nm min^{-1}.

2.2. LiPONB thin film deposition

LiPONB electrolyte film was deposited by radio-frequency (rf) reactive sputtering at a power density of 2.0 W cm^{-2} using a (Li_3PO_4–$LiBO_2$ 95/5) target in a pure nitrogen atmosphere under a total nitrogen pressure of 2 Pa. Before deposition, a vacuum was applied into the chamber until the pressure was less than 4×10^{-6} Pa. Prior to each deposition, a pre-sputtering was systematically carried out for 20 min. The growth rate of the LiPONB deposit was determined equal to 5 nm min^{-1}.

2.3. Li thin film deposition

Metallic Li was deposited by thermal evaporation with a growth rate of 150 nm min^{-1}.

2.4. Fabrication of the thin-film microbattery

The all-solid-state TiOS/LiPONB/Li microbatteries were prepared as follows at the pilot scale using an ENDURA sputtering platform (Applied Materials). The 6″ or 8″ silicon wafers used as substrates were successively covered by an insulating SiO_x film, a barrier film to avoid any lithium diffusion into the substrate and a 200 nm tungsten level patterned by photolithography as a current collector (Fig. 1). The deposition of the following levels of the stack was made through a shadow mask in order to localize each layer. TiO_yS_z thin films with a thickness of 1.3 μm were grown by DC sputtering on the current collector. The LiPONB solid electrolyte film, 1.4 μm thick, was then deposited by rf reactive sputtering under a

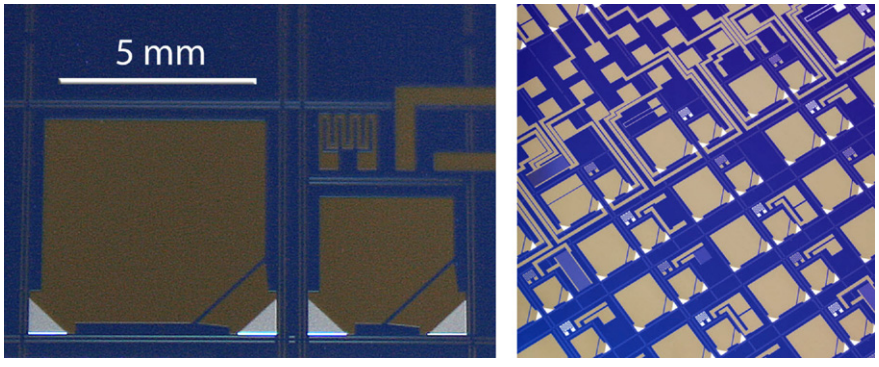

Fig. 1. W current collector level on a silicon wafer showing the different sizes of microbatteries (25 and 7 mm^2).

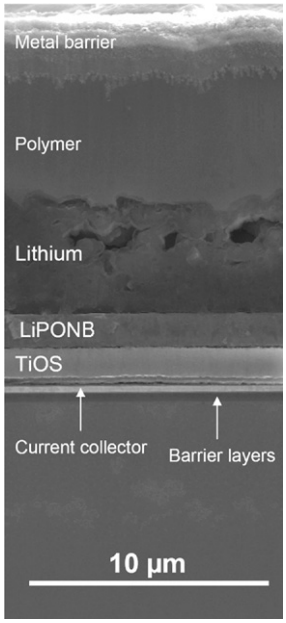

Fig. 2. SEM cross-section image of an all-solid-state microbattery.

pure nitrogen atmosphere. To complete the active part of the microbattery, a metallic lithium film, 3 μm thick, was then deposited on the LiPONB film by thermal evaporation. To protect the active stack from moisture and oxygen, an encapsulation based on a polymer/metal multilayer was achieved by chemical vapor deposition and sputtering. A SEM picture of the cross-section showing all the films constituting the stack is shown in Fig. 2. On each silicon wafer, microbatteries with surface areas equal to 7 or 25 mm^2 were prepared (Fig. 1).

2.5. Characterizations of the active material thin films

To avoid any contamination, air-tight containers were systematically used to transfer the sample from the sputtering chamber to the various characterization apparatus.

The chemical composition of the TiO_ySz thin film positive electrode was determined by Rutherford backscattering spectroscopy (RBS) at a backscattering angle of 150° using an incident beam of $^4He^+$ ions with an energy of 2 MeV. The spectra were analyzed with the SIMNRA software [10]. For that purpose, the 100 nm thin films were deposited onto vitreous carbon substrates. The composition homogeneity over the thickness was checked by Auger electron spectroscopy (VG Microlab 310 F) on thin films deposited onto standard silicon wafers and having a thickness of 1.3 μm.

The structure was studied by means of X-ray diffraction (Philips PW 1050, Cu Kα radiation).

The thickness, surface and cross-section morphology were investigated using a Tencor profilometer alpha-step 200 and scanning electron microscopy (JEOL-JSM 6360). The X-ray photoelectron spectroscopy (XPS) was performed with a KRATOS (model Axis ultra 165) using a monochromatized Al Kα radiation (1486.7 eV). The residual pressure inside the analysis chamber was in the 5×10^{-9} Pa range. The spectrometer was calibrated using the photoemission lines of gold (Au $4f_{7/2}$ = 83.9 eV, with reference to the Fermi level) and copper (Cu $2p_{3/2}$ = 932.5 eV). For the Au $4f_{7/2}$ lines, the full width at half maximum (FWMH) was 0.86 eV. The peaks were recorded with a constant pass energy of 50 eV. All the samples were fixed on the sample holders in a glove box directly connected to the introduction chamber of the spectrometer. The XPS analyses were carried out on the as-deposited thin film. Peaks were then shifted to align the hydrocarbon C1s photoemission line to 285.0 eV binding energy. The experimental curves were fitted with a combination of Gaussian (80%) and Lorentzian (20%) functions using a minimum number of components.

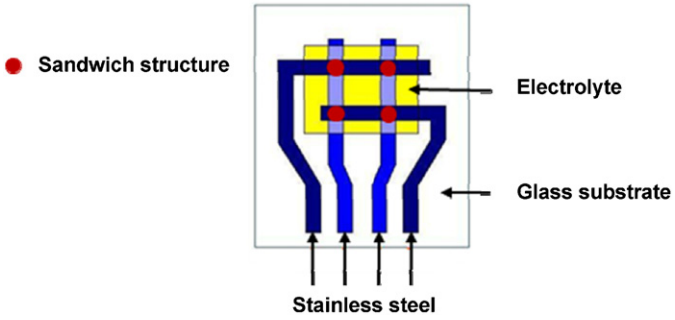

Fig. 3. Stainless steel/electrolyte/stainless steel sandwich structures used for the determination of ionic conductivity by impedance spectroscopy. This design allows four measurements for each thin film electrolyte in order to ensure a good accuracy.

The chemical composition of LiPONB thin films was determined by RBS and electron microprobe analysis (Cameca SX100) for P, O and N contents. The Li, B and P contents were determined using an inductively coupled plasma-optical emission spectrometer (ICP-OES) (Varian 720ES) by firstly dissolving thin films deposited on the glass substrate in 10 ml of diluted HCl. A small quantity of these solutions was injected. The wavelength of the emission line is 460.289 nm for Li, 214.914 nm for P and 249.678 nm for B.

The ionic conductivity of LiPONB thin films was measured by impedance spectroscopy using a Solartron 1260 analyzer. Stainless steel/electrolyte/stainless steel sandwich structures were prepared on glass substrates. A special design with a grid allowing 4 measurements for each thin film electrolyte was used to ensure the reproducibility and the accuracy of the results. The overlap area of each plot was 4 mm^2 (Fig. 3). The stainless steel electrodes were deposited by radio-frequency magnetron sputtering from a stainless steel target under a pure argon atmosphere. The impedance measurements were carried out in a frequency range from 1 Hz to 10 MHz with 50 mV AC voltage amplitude with a 5 °C increment from 30 °C to 75 °C. The ionic conductivity, σ, was calculated from the following equation:

$$\sigma = \frac{1}{R}\frac{d}{A}$$

where d is the solid electrolyte thin film thickness, A is the area of the electrode and R is the resistance of the solid electrolyte thin film deduced from the Nyquist diagram. The local structure of LiPONB was investigated by X-ray photoelectron spectroscopy (XPS) and TEM.

2.6. Electrochemical characterization of the Li/LiPONB/TiO_ySz microbattery

Electrochemical measurements were conducted using a VMP3 galvanostat-potentiostat (Bio-Logic) with channels equipped for electrochemical impedance spectroscopy (EIS) analysis. The microbatteries were connected using a probehead with multiple gold plated tips and placed at 20 °C in a thermostated chamber. Different cells of a given wafer were used for each type of experiment.

Various electrochemical characterizations were achieved including galvanostatic cycling between 1 V and 3 V/Li^+/Li, cyclic voltammetry at a low sweep rate of 5 μV s^{-1}, Galvanostatic Intermittent Titration Technique (GITT) and EIS analyses. Note that a relaxation time of 1 h was applied before impedance measurements. The lithium chemical diffusion coefficient was calculated from GITT measurements for various Li_xTiO_ySz compositions using

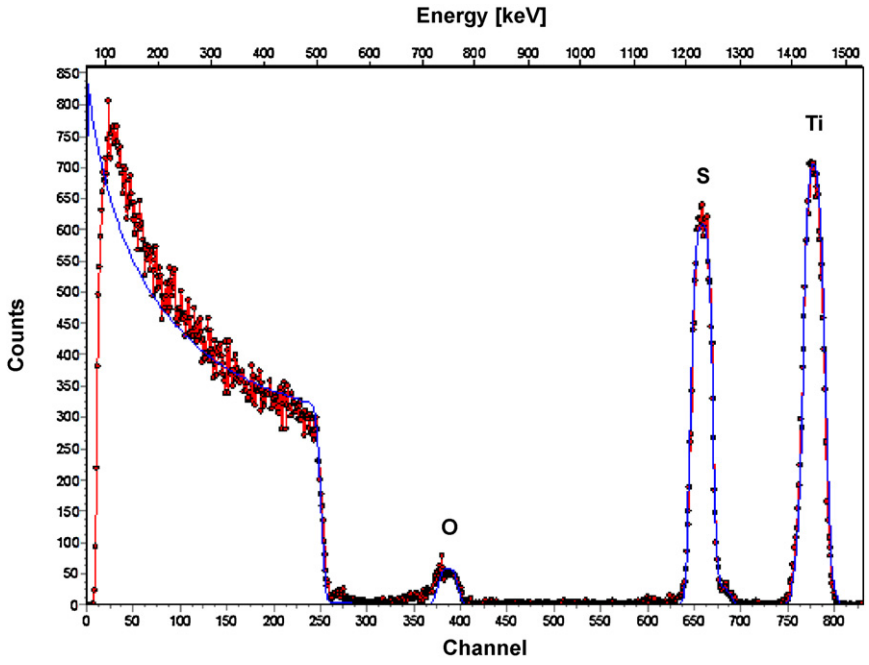

Fig. 4. RBS analysis of a TiOS thin film electrode 100 nm thick deposited on vitreous carbon. The composition deduced from the fit (line) done with SIMNRA [10] is $TiO_{0.6}S_{1.6}$.

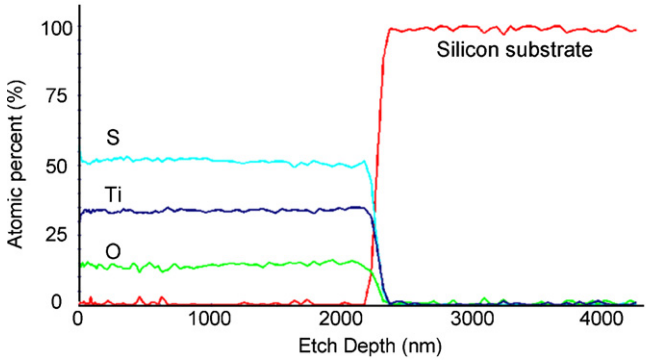

Fig. 5. AES analysis of a TiOS thin film electrode deposited on silicon wafer in depth profile.

the method described by Weppner [11] according to the following equation:

$$\tilde{D} = \frac{4}{\pi}\left(\frac{V_M i_0}{F}\right)^2 \left[\frac{dE/dx}{(dE/d\sqrt{t})}\right]^2$$

V_M is defined as the molar volume, i_0 is the applied constant current density, F is Faraday's constant (96500 C), E is the cell voltage and x is the stoichiometric number of lithium. The lithium content in the lithiated titanium oxysulfide thin film of the all-solid-state microbatteries was deduced from previous measurements made on weighted TiO_yS_z thin films cycled in liquid electrolyte. The sequence used for the galvanostatic intermittent titration can be described as follows: a constant current density ($i_0 = \pm 10\ \mu A\ cm^{-2}$) was applied for a given time leading to constant charge increments $\Delta x = \pm 0.025$, followed by a 4 h rest period.

3. Results and discussion

3.1. Individual thin films

The chemical composition of the positive electrode thin film determined by RBS spectroscopy was $TiO_{0.6}S_{1.6}$ (Fig. 4). Auger spectroscopy revealed a uniform composition over the whole thickness for all samples, in agreement with the composition determined by RBS spectroscopy (Fig. 5). XRD and TEM analyses showed that TiOS thin films were amorphous. The surface and cross-section SEM images are presented in Fig. 6a and b. The surface was homogeneous and composed of grains with a diameter in the order of 200 nm (Fig. 6a). The image of the cross-section showed a typical columnar growth (Fig. 6b), similar to the TiOS thin films previously studied by Lindic et al. [12]. The Ti2p and S2p XPS spectra corresponding to $TiO_{0.6}S_{1.6}$ thin films are very close to that previously published by Lindic et al. (see Refs. [6,8]). More precisely, the Ti2p3/2–1/2

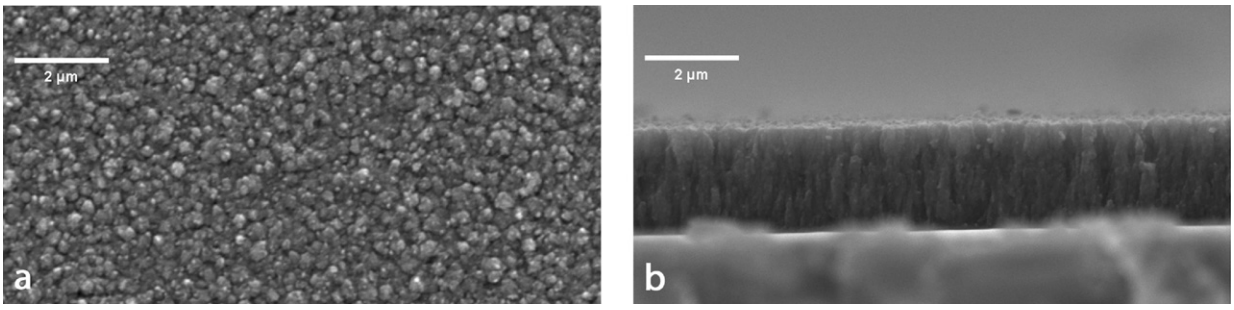

Fig. 6. SEM images of a TiOS thin film electrode. (a) Surface and (b) cross-section.

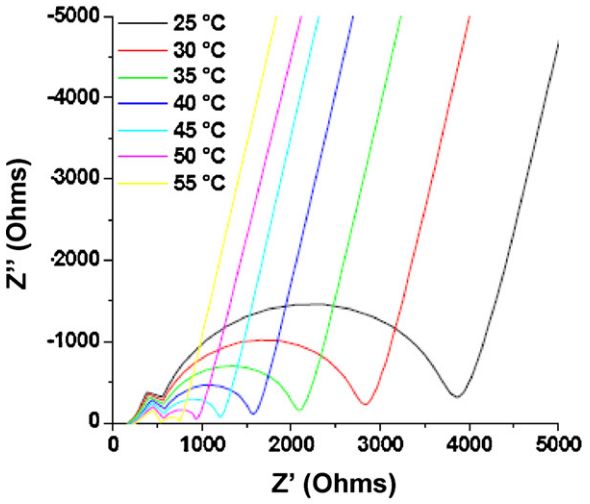

Fig. 7. Impedance measurements on the LiPONB thin film electrolyte at various temperatures from 25 °C to 55 °C.

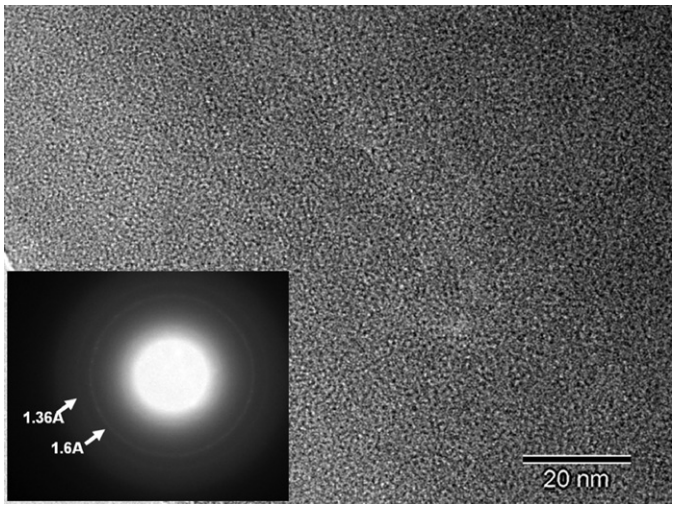

Fig. 8. TEM image of LiPONB thin film showing its amorphous state.

XPS core peak may be fitted into two doublets: the first one, with the main intensity (89%), is located at 456.3–462.3 eV and corresponds to Ti^{4+} ions in a sulfur environment as in TiS_2 reference (456.1–462.2 eV) or in TiS_3 (456.0–462.2 eV). The second one (11%) is assigned to Ti^{4+} ions in a majority oxygen environment since the binding energy (458.1–463.8 eV) is close the rutile TiO_2 reference (458.5–464.1 eV). The relative percentages of the doublet area clearly reveal the prevalence of Ti^{4+} ions in a sulfur environment.

The S2p3/2–1/2 XPS core peak was fitted into two components, assigned to the presence of S_2^{2-} disulfide pairs located at 162.3–163.5 eV as in TiS_3 reference (162.3–163.4 eV) in addition to S^{2-} at 161.1–162.3 eV (as in TiS_2 – 160.9–162.1 eV – or TiS_3 – 161.0–162.1 eV – references). Note that S^{2-} ions are present in the thin film with a higher proportion (70%) than S_2^{2-} disulfide pairs (30%), but the presence of those has a great importance regarding to the redox processes in agreement with the previous studies of Lindic et al.

The composition of LiPONB thin films determined by three complementary techniques, RBS spectroscopy and electron microprobe analysis for P, O and N amounts and ICP for Li/P and Li/B ratios was $Li_{3.64}PO_{3.63}N_{0.46}B_{0.07}$. The ionic conductivity was deduced from impedance measurements carried out on the following stack: blocking electrode/LiPONB/blocking electrode. At room temperature, the ionic conductivity was equal to 2.6×10^{-6} S cm^{-1} (Fig. 7). The activation energy was determined equal to 0.63 eV from ionic conductivity measurements taken at various temperatures according to the Arrhenius law. The local structure was investigated by TEM and XPS spectroscopy. TEM analysis has confirmed the amorphous nature of the electrolyte (Fig. 8).

The spectrum of the N1s core peak (Fig. 9) was decomposed into two Gaussian–Lorentzian mixed components respectively located at 397.8 eV and 399.4 eV (±0.1 eV) in agreement with the studies of Marchand et al. [13]. These two values of binding energies can be attributed to two different bonding states of nitrogen atoms. The first one, labeled N1, is bound to two phosphorus atoms (–N=), while the second one N2 corresponds to a nitrogen atom linked to three phosphorus atoms (–N<). The energy difference of 1.6 eV observed between the two peaks is consistent with the results obtained for a $P_3N_5H_x$ phosphorus nitride [14] in which these two nitrogen chemical environments also exist. For the latter, the reported values of binding energies are respectively 397.0 eV and 398.6 eV. The shift towards higher energies compared to the Veprek et al. results could be interpreted by the presence of oxygen bound to phosphorus, in agreement with an initial state effect.

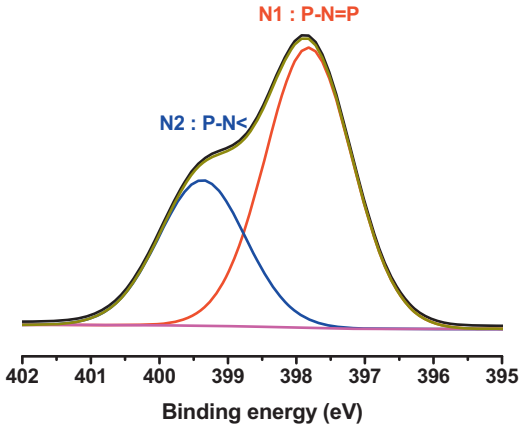

Fig. 9. N1s XPS spectrum of LiPONB thin film electrolyte.

3.2. Electrochemical behavior of all-solid-state microbatteries

At room temperature, the sweep voltammogram of the microbattery (Fig. 10) achieved at low rate (5 μV s^{-1}) exhibited two defined regions in the range [1.8–3.0 V] and [1.0–1.8 V Vs Li/Li$^+$] corresponding to the reversible reduction of respectively S_2^{2-} and

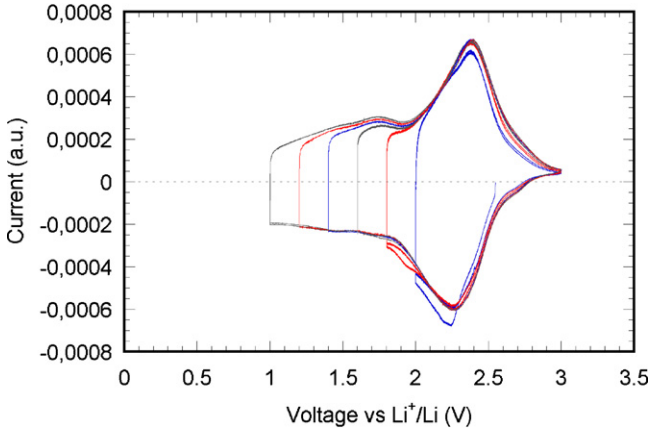

Fig. 10. Linear sweep voltammograms of TiOS/LiPONB/Li cell done at a scan rate of 5 μV s^{-1} between 3 V for the upper limit and various lower cut off voltages from 2 V to 1 V. Two cycles were done for each potential range.

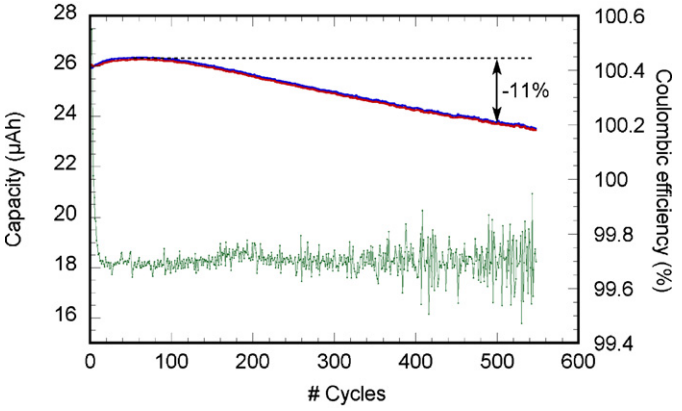

Fig. 11. Evolution of both capacity and coulombic efficiency of a 25 mm^2 cell cycled at a constant current density (100 µA cm^{-2}) between 1 V and 3 V. The thickness of the positive electrode is around 1.2 µm.

Ti^{4+}. These two reduction/oxidation steps have been confirmed by XPS measurements at the S2p and Ti2p core peaks achieved on TiOS electrodes cycled in liquid electrolyte. During galvanostatic cycling at 100 µA cm^{-2} between 1.0 and 3.0 V, the 25 mm^2 Li/LiPONB/TiOS cell exhibited a high volumetric capacity close to 90 µAh cm^{-2} µm^{-1}, which is 38% greater than the theoretical value of $LiCoO_2$ (65 µAh cm^{-2} µm^{-1}) which is commonly used as a positive electrode in all-solid-state lithium microbatteries (Fig. 11). In addition, the Li/LiPONB/TiOS cell had an excellent cycle life with a corresponding fading rate of −0.02% per cycle. After 500 cycles, only a minor evolution of the voltage versus capacity curve is observed in the region corresponding to the oxidation of S^{2-} species (Fig. 12a and b).

The chemical lithium diffusion coefficient was calculated from GITT experiments at 20 °C using an estimated molar volume of 32.3 cm^3 mol^{-1} for $TiO_{0.6}S_{1.6}$. The slope $dE/d(\sqrt{t})$ was determined for a period of time comprised between 2 and 10 s for each current pulse. This coefficient ranged mainly from 5×10^{-11} to 3×10^{-10} cm^2 s^{-1} between the compositions $TiO_{0.6}S_{1.6}$ and $Li_{1.2}TiO_{0.6}S_{1.6}$ (Fig. 13) which was rather high in this disordered insertion material compared to the values measured on crystalline materials such as $LiCoO_2$ (10^{-13}–10^{-11} cm^2 s^{-1}) [15] or $LiMn_2O_4$ (10^{-12}–10^{-10} cm^2 s^{-1}) [16].

An estimation of the maximum value of the self-discharge was carried out by measuring the evolution of the OCV (open circuit voltage). The drift of the OCV is due both to the homogenization of concentration profiles and to the self-discharge of the cell. The latter being preponderant after 20 days was estimated at around −12 µV h^{-1} (corresponding to −5.2% per year) by the measurement of the OCV drift in the charged state (Fig. 14). Even if this method leads to an overestimation of the self-discharge, the direct measurement by storing a charged cell knowing its initial reversible capacity during one year is not adapted to industrial test specifications. Moreover, the obtained value is much lower than the specified value for the envisaged applications.

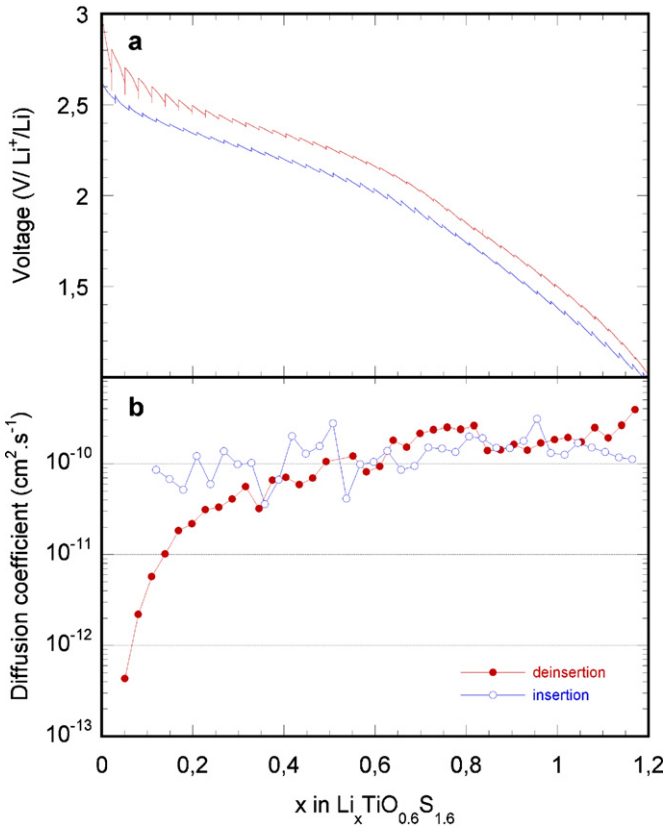

Fig. 13. (a) Galvanostatic intermittent titration performed both in charge and in discharge on a two electrodes 7 mm^2 all-solid-state cell, and (b) the deduced variation of lithium chemical diffusion coefficient with the lithium content in Li_xTiOS. The estimated thickness of the TiOS thin film is 1.0 µm.

The impedance measurement analysis carried out at the end of each charge and discharge showed progressive modifications over cycles. Hence, the internal resistance of the Li/LiPONB/TiOS

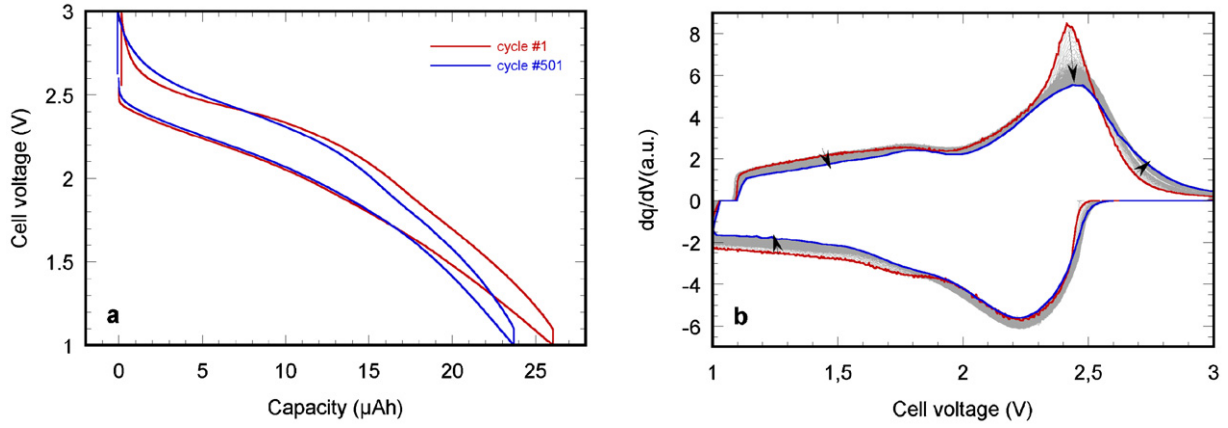

Fig. 12. (a) Evolution of the voltage–capacity curve after 500 cycles. Charges and discharges have been done at a constant current density of 100 µA cm^{-2}. (b) Evolution of the corresponding incremental capacity over 500 cycles showing a slight evolution of the S^{2-} oxidation step at 2.4 V.

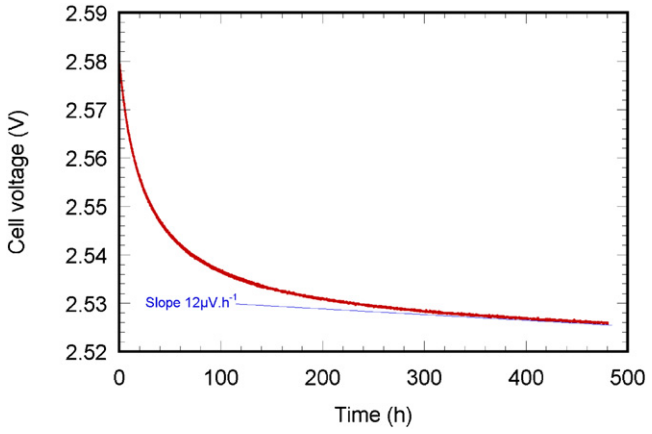

Fig. 14. Evolution of the open circuit voltage of a fully charge cell (3 V/Li^+/Li).

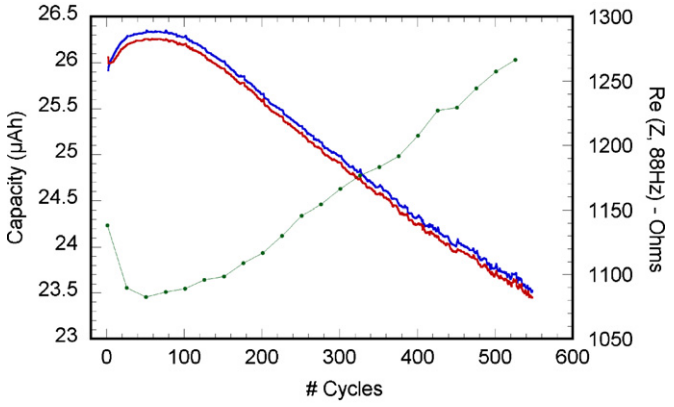

Fig. 15. Correlation of the capacity fading with the increase of the cell impedance measured at 88 Hz.

cell increased whereas the capacity decreased (Fig. 15). A correlation has been established between the capacity fading and the cell impedance increase. The evolution of the real and the imaginary part of the impedance at the end of the charge between the first and the 501th cycle are plotted in Fig. 16. The evolution of the cell impedance does not involve a new limiting step that could correspond to the formation of a new interface but is only increased by a real scale factor. In addition, the relaxation frequency characteristic of the solid electrolyte remains unchanged over cycles. So, to explain this impedance increase observed for

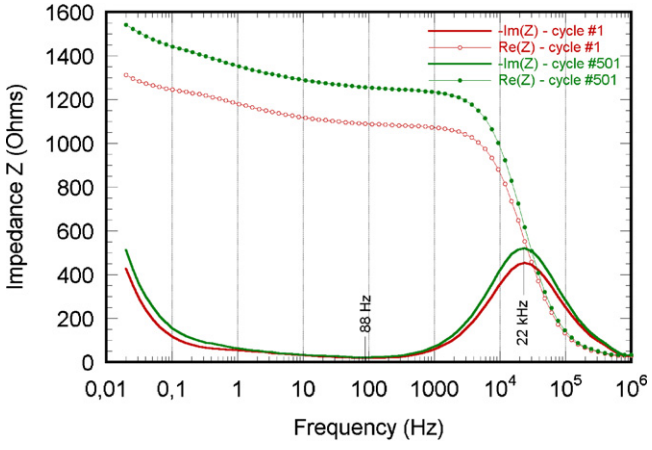

Fig. 16. Evolution with frequency of the real and the imaginary part of the impedance for the 1st cycle and the 501th cycle.

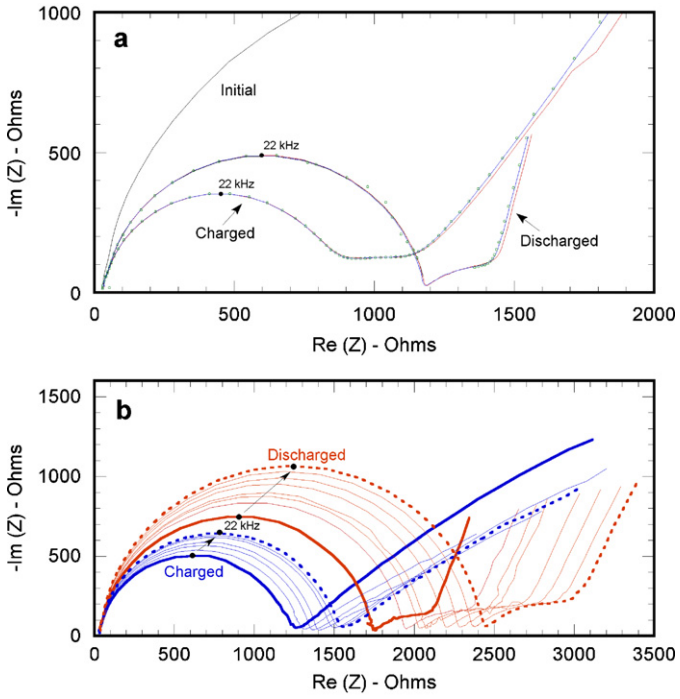

Fig. 17. Evolution of the impedance spectra for cells discharged at 10 µA cm^{-2} and charged either at 10 µA cm^{-2} (a) or 200 µA cm^{-2} (b).

solid-state microbatteries having a planar geometry, the most obvious hypothesis would be to consider a modification of the negative or positive electrode/solid contact area. To try to identify the origin of a such increase, complementary impedance analyses were carried out by measuring the evolution of the cell impedance for different values of the charge current while maintaining the discharge current at 10 µA cm^{-2} (Fig. 17). At a low charge current density (10 µA cm^{-2}), the impedance was fully stable either in the charged or in the discharged states. Nevertheless, during the discharge, we observed a second half-circle at low frequency which could correspond to the formation of an interface between the LiPONB solid electrolyte and the TiOS positive electrode. At a charge current density of 100 µA cm^{-2}, the impedance rapidly increased during the first cycles and then roughly stabilized. The impedance dramatically increased during charge and discharge for the charge current density of 200 µA cm^{-2} while maintaining the discharge current at 10 µA cm^{-2} as for the other analyses. Thus, the results of these experiments carried out with various charge current densities while maintaining a low discharge current density (10 µA cm^{-2}) show that the main origin of the impedance increase is linked to the current density. All these results would tend to indicate that the main origin of the capacity fading is related to a modification of the morphology of the Li electrode during charging which induced a progressive decrease of the Li/LiPONB contact area and an increase of the internal resistance during subsequent discharges. This explanation is not so surprising if we consider a previous study leaded by J.B. Neudecker on Li-free microbattery showing that the Li deposit after a charge is not necessary homogeneous and can form some nodules at the electrode/electrolyte interface which limits the Li/solid electrolyte contact area [17].

4. Conclusion

The all-solid-state Li/LiPONB/TiOS cells produced at the pilot scale exhibit excellent performances in terms of cycle life, efficiency and self-discharge in the operating range [1–3 V]. The use of lower charge current densities (lower than 100 µA cm^{-2}) guarantees a

cycle life superior to 1000 cycles at 100% depth of discharge. The progressive capacity loss of around 0.02% per cycle correlated with a low increase of the cell impedance, is related to the evolution of the Li/LiPONB interface for higher values of the charge current density. The characteristics of these cells make them an excellent miniaturized secondary energy source for numerous applications for which compatibility with the solder-reflow operation is not compulsory.

Acknowledgements

The authors would like to thank the Agence Nationale de la Recherche for its financial support through the ANR project Mat&Pro 'EFIMI' and Stéphanie Sorieul from AIFIRA for her help in acquiring RBS spectra.

References

[1] J.B. Bates, G.R. Gruzalski, N.J. Dudney, C.F. Luck, X. Yu, Proc. 8th Electronic Materials and Processing Congress, 30 August–2 September, San Jose, CA, USA, 1993.
[2] J.B. Bates, N.J. Dudney, D.C. Lubben, G.R. Gruzalski, S.B. Kwak, X. Yu, R.A. Zuhr, J. Power Sources 54 (1995) 58–62.
[3] Y. Iriyama, K. Nishimoto, C. Yada, T. Abe, Z. Ogumi, K. Kikuchi, J. Electrochem. Soc. 153 (2006) A821–A825.
[4] C. Navone, R. Baddour-hadjean, J.P. Pereira-Ramos, R. Salot, J. Electrochem. Soc. 156 (2009) A763–A767.
[5] A. Gies, B. Pecquenard, A. Benayad, H. Martinez, D. Gonbeau, H. Fuess, A. Levasseur, Solid State Ionics 176 (2005) 1627–1634.
[6] M.H. Lindic, B. Pecquenard, P. Vinatier, A. Levasseur, H. Martinez, D. Gonbeau, P.E. Petit, G. Ouvrard, J. Electrochem. Soc. 152 (2005) A141–A146.
[7] A. Levasseur, G. Meunier, R. Dormoy, Pat. WO9005387 (1988).
[8] M.H. Lindic, H. Martinez, A. Benayad, B. Pecquenard, P. Vinatier, A. Levasseur, D. Gonbeau, Solid State Ionics 176 (2005) 1529–1537.
[9] M. Martin, O. Blandenet, Pat. WO2005050764 (2005).
[10] W. Eckstein, M. Mayer, Nucl. Instrum. Methods B 153 (1999) 337.
[11] W. Weppner, R.A. Hugghins, J. Electrochem. Soc. 124 (1977) 1569.
[12] M.H. Lindic, B. Pecquenard, P. Vinatier, A. Levasseur, H. Martinez, D. Gonbeau, P.E. Petit, G. Ouvrard, Thin Solid Films 484 (2005) 113–123.
[13] R. Marchand, D. Agliz, L. Boukbir, A. Quemerais, J. Non-Cryst. Solids 103 (1988) 35–44.
[14] S. Veprek, Z. Iqbal, J. Brunner, M. Schärli, Philos. Mag. B 43 (1981) 527–547.
[15] H. Xia, L. Lu, G. Ceder, J. Power Sources 159 (2006) 1422–1427.
[16] J. Xie, T. Tanaka, N. Imanishi, T. Matsumura, A. Hirano, Y. Takeda, O. Yamamoto, J. Power Sources 180 (2008) 576–581.
[17] B.J. Neudecker, N.J. Dudney, J.B. Bates, J. Electrochem. Soc. 147 (2000) 517–523.